The Journal of Immunology

Atypical Activin A and IL-10 Production Impairs Human CD16 $^{+}$ Monocyte Differentiation into Anti-Inflammatory Macrophages

Érika González-Domínguez, Ángeles Domínguez-Soto, Concha Nieto, José Luis Flores-Sevilla, Mariana Pacheco-Blanco, Victoria Campos-Peña, Marco A. Meraz-Ríos, Miguel A. Vega, Ángel L. Corbí and Carmen Sánchez-Torres

J Immunol published online 4 January 2016
http://www.jimmunol.org/content/early/2016/01/02/jimmunol.1501177

The Journal of Immunology is published twice each month by The American Association of Immunologists, Inc., 9650 Rockville Pike, Bethesda, MD 20814-3994.

Print ISSN: 0022-1767 Online ISSN: 1550-6606.

Published January 4, 2016, doi:10.4049/jimmunol.1501177

Atypical Activin A and IL-10 Production Impairs Human CD16$^+$ Monocyte Differentiation into Anti-Inflammatory Macrophages

Érika González-Domínguez,* Ángeles Domínguez-Soto,† Concha Nieto,† José Luis Flores-Sevilla,* Mariana Pacheco-Blanco,*,[1] Victoria Campos-Peña,‡ Marco A. Meraz-Ríos,* Miguel A. Vega,† Ángel L. Corbí,†,[2] and Carmen Sánchez-Torres*,[2]

Human CD14^{++}CD16$^-$ and CD14$^{+/lo}$CD16$^+$ monocyte subsets comprise 85 and 15% of blood monocytes, respectively, and are thought to represent distinct stages in the monocyte differentiation pathway. However, the differentiation fates of both monocyte subsets along the macrophage (Mϕ) lineage have not yet been elucidated. We have now evaluated the potential of CD14^{++} CD16$^-$ and CD16$^+$ monocytes to differentiate and to be primed toward pro- or anti-inflammatory Mϕs upon culture with GM-CSF or M-CSF, respectively (subsequently referred to as GM14, M14, GM16, or M16). Whereas GM16 and GM14 were phenotypic and functionally analogous, M16 displayed a more proinflammatory profile than did M14. Transcriptomic analyses evidenced that genes associated with M-CSF–driven Mϕ differentiation (including *FOLR2*, *IL10*, *IGF1*, and *SERPINB2*) are underrepresented in M16 with respect to M14. The preferential proinflammatory skewing of M16 relative to M14 was found to be mediated by the secretion of activin A and the low levels of IL-10 produced by M16. In fact, activin A receptor blockade during the M-CSF–driven differentiation of CD16$^+$ monocytes, or addition of IL-10–containing M14-conditioned medium, significantly enhanced their expression of anti-inflammatory–associated molecules while impairing their acquisition of proinflammatory-related markers. Thus, we propose that M-CSF drives CD14^{++}CD16$^-$ monocyte differentiation into bona fide anti-inflammatory Mϕs in a self-autonomous manner, whereas M-CSF–treated CD16$^+$ monocytes generate Mϕs with a skewed proinflammatory profile by virtue of their high activin A expression unless additional anti-inflammatory stimuli such as IL-10 are provided. ***The Journal of Immunology*****, 2016, 196: 000–000.**

Monocytes are blood-borne cells that can migrate to tissues and give rise to dendritic cells and macrophages (Mϕs) in the steady-state and in pathological conditions (1). Based on CD14 and CD16 expression, two major subsets of human circulating monocytes have been defined. The classical CD14^{++}CD16$^-$ cell subset accounts for 85–90% of total monocytes, whereas the minor CD16$^+$ monocyte subpopulation comprises the remaining 10–15% (2) and is further subdivided into intermediate CD14^{++}CD16$^+$ and nonclassical CD14$^+$CD16^{++} monocytes (3). The present concept is that these monocyte subsets represent distinct developmental stages, with the intermediate subset being the direct intermediary link between the immature classical and the more mature nonclassical monocyte subsets (2), and that M-CSF contributes to this differentiation (4, 5). Functional studies have shown that CD16$^+$ monocytes are the main source of TNF and IL-1β upon TLR-2, -4, -7, or -8 stimulation (6–8). Moreover, their blood numbers significantly increase in chronic inflammatory conditions (9). Together with their reduced ability to produce IL-10 (10), these data led to the conclusion that CD16$^+$ monocytes are potent inducers of inflammation (7, 11).

Tissue Mϕs are heterogeneous with respect to phenotype and function. In tissues, Mϕs undergo genetic reprogramming in response to environmental signals that drive Mϕ differentiation toward a variety of functional phenotypes, where M1 (classical) and M2 (alternative) Mϕs represent the endpoints of the activation spectrum. M1 Mϕs primarily exhibit proinflammatory abilities,

*Departamento de Biomedicina Molecular, Centro de Investigación y de Estudios Avanzados del Instituto Politécnico Nacional, 07360 Mexico City, Mexico; †Laboratorio de Células Mieloides, Departamento de Microbiología Molecular y Biología de las Infecciones, Centro de Investigaciones Biológicas, Consejo Superior de Investigaciones Cientificas, 28040 Madrid, Spain; and ‡Laboratorio Experimental de Enfermedades Neurodegenerativas, Instituto Nacional de Neurología y Neurocirugía "Manuel Velazco Suárez," 14269 Mexico City, Mexico

[1]Current address: Vascular Cell Biology Department, Max Planck Institute for Molecular Biomedicine, Münster, Germany.

[2]Á.L.C. and C.S.-T. are cosenior authors.

ORCIDs: 0000-0001-7404-0038 (É.G.-D.); 0000-0003-2930-342X (M.P.-B.); 0000-0001-8282-7543 (V.C.-P.); 0000-0001-6748-8117 (M.A.M.-R.).

Received for publication May 22, 2015. Accepted for publication November 23, 2015.

This work was supported by Mexican Secretaría de Educación Pública–Consejo Nacional de Ciencia y Tecnología Grant 179388 (to C.S.-T.) and Spanish Ministerio de Economía y Competitividad Grant SAF2014-52423-R (to Á.L.C.). É.G.-D., J.L.F.-S., and M.P.-B. were the recipients of Consejo Nacional de Ciencia y Tecnología Scholarships 302832, 322167, and 245016, respectively.

The microarray data presented in this article have been submitted to the Gene Expression Omnibus (http://www.r-project.org) under accession number GSE68061.

Address correspondence and reprint requests to Dr. Carmen Sánchez-Torres, Departamento de Biomedicina Molecular, Centro de Investigación y de Estudios Avanzados del Instituto Politécnico Nacional, Avenida Instituto Politécnico Nacional 2508, 07360 Mexico City, Mexico. E-mail address: csanchez@cinvestav.mx

The online version of this article contains supplemental material.

Abbreviations used in this article: FR, folate receptor; GM14, CD14^{++}CD16$^-$ monocyte-derived Mϕ generated with GM-CSF; GM16, CD16$^+$ monocyte-derived Mϕ generated with GM-CSF; GM-Mϕ, monocyte-derived Mϕ generated with GM-CSF; GO, gene ontology; GSEA, gene set enrichment analysis; HO-1, heme-oxygenase 1; IRF, IFN regulatory factor; Mϕ, macrophage; M14, CD14^{++}CD16$^-$ monocyte-derived Mϕ generated with M-CSF; M16, CD16$^+$ monocyte-derived Mϕ generated with M-CSF; M-Mϕ, monocyte-derived Mϕ generated with M-CSF; PPAR, peroxisome proliferator–activated receptor; qRT-PCR, RT-quantitative real-time PCR; SN, supernatant; TF, transcription factor.

whereas M2 Mϕs mainly exert anti-inflammatory and immunoregulatory activities (12). The high functional and phenotypic plasticity of Mϕs is illustrated by the fact that their polarization can be reversed both in vitro and in vivo (13, 14). Prototypic polarizing stimuli are IFN-γ and LPS (M1) and IL-4, immune complexes, or IL-10 (M2) (12). Mϕ polarization is also modulated by GM-CSF (toward M1) and M-CSF (toward M2) (13, 15, 16).

Two major monocyte subpopulations can be identified in mice. The "inflammatory" CCR2^{hi}Ly6C^{hi} subset resembles human CD14^{++}CD16$^-$ monocytes, whereas the "resident/patrolling" CCR2^{lo}Ly6C^{lo} subset shares some features with human CD16$^+$ monocytes (6, 17–19). The functional commitment of the distinct mouse monocyte subsets has been addressed, and controversial results have been reported relating their fate and extravasation capacity toward damaged tissues. Several studies indicate that both Ly6C^{hi} and Ly6C^{lo} monocytes are recruited to injured or inflamed sites in diverse pathological settings. There, they initiate a genetic program associated with recruitment of new inflammatory cells and recognition and elimination of microorganisms (M1), whereas later they contribute to wound healing by acquiring a proresolution phenotype (M2) (20–23). Others have proposed that Ly6C^{hi} monocytes selectively give rise to M1 Mϕs and, conversely, Ly6C^{lo} monocytes become M2 Mϕs (24, 25). Indeed, although Ly6C^{hi} monocytes are prone to arrive to inflammatory sites by virtue of their high CCR2 expression (17, 26), their differentiation into M1 or M2 Mϕs might vary according to the type of immune response in the affected tissue (i.e., type I or type II inflammation) (27).

Previous studies have analyzed the polarization of human CD14$^+$ monocyte-derived Mϕs (15, 16). However, the differentiation potential of the two main human monocyte subtypes into pro- and anti-inflammatory Mϕs has not yet been elucidated. The present study was undertaken to investigate whether the CD14^{++} CD16$^-$ and CD16$^+$ monocyte subsets are already skewed in their Mϕ polarization potential.

Materials and Methods

Media and reagents

Monocytes were cultured in RPMI 1640 supplemented with 10% FCS, 2 mM L-glutamine (HyClone Laboratories, Logan, UT), and 1% penicillin/streptomycin (Life Technologies, Grand Island, NY). The following reagents were used: human GM-CSF (1000 U/ml, provided by Probiomed, Mexico City, Mexico); M-CSF (10 ng/ml) and IL-10 (20 ng/ml) (R&D Systems, Minneapolis, MN); rat neutralizing mAb to IL-6 and to IL-10 (5 μg/ml), murine neutralizing mAb to TNF (5 μg/ml), and their respective Ig isotype controls (BD Biosciences, Bedford, MA); murine neutralizing mAb to TGF-β1 (R&D Systems, 1 μg/ml); A83-01 (1 μM, Tocris Bioscience, Bristol, U.K.); and LPS (*Escherichia coli* 0111:B4, 10 ng/ml, Sigma-Aldrich, St. Louis, MO).

Monocyte subset isolation and differentiation into macrophages

Human PBMCs were obtained by Ficoll density gradient (Nycomed Pharma, New York, NY) of buffy coats from healthy donors. CD14^{++} CD16$^-$ and CD16$^+$ monocytes were purified by positive selection using magnetic separation systems (MACS, Miltenyi Biotec, Auburn, CA), as previously reported (28). These procedures routinely provided 70–95% pure monocytes. Cells were cultured at 0.5×10^6 cells/ml for 6 d in complete medium containing GM-CSF or M-CSF to generate GM-Mϕs and M-Mϕs, respectively. GM-Mϕs derived from CD14^{++} CD16$^-$ and CD16$^+$ monocytes are subsequently referred to as GM14 and GM16, respectively, whereas M-Mϕs derived from CD14^{++} CD16$^-$ and CD16$^+$ monocytes are referred to as M14 and M16, respectively.

The cultures were fed with cytokines every 2 d. In some experiments, cells were cultured with the inhibitor of ALK-4, -5, and -7 A83-01 (added every day). mAbs against different cytokines and their respective Ig isotype controls were added from the beginning of cultures and maintained throughout the Mϕ differentiation process. Supernatants (SNs) from M-Mϕs were collected every day, starting at first day of culture, and stored at −80°C until use. They were added at 50% (v/v) to monocytes differentiated with M-CSF from the first day of culture onward.

Flow cytometry assays

Phenotypic analyses were carried out by indirect immunofluorescence using unlabeled primary mAbs directed against human CD1a, CD14, and CD209 (all from BD Biosciences), CD163 and CLEC5A (R&D Systems), GM-CSF receptor (CD116, BioLegend, San Diego, CA), and folate receptor (FR)β (29), followed by incubation with Cy5-labeled goat anti-mouse Igs. Staining was performed in the presence of 50 μg/ml human IgG. The proper Ig isotypes were included as negative controls. Data were acquired in a FACSCalibur (BD Biosciences).

Proliferation assays

Allogeneic CD4$^+$ T lymphocytes were isolated by negative selection using the MACS CD4$^+$ T cell isolation kit (Miltenyi Biotec), followed by incubation with MACS anti-CD45RO Abs to obtain naive CD45RA$^+$ cells. CD4$^+$CD45RA$^+$ T cells were labeled with CFSE (10 μM, Molecular Probes, Eugene, OR). Then, T cells were cocultured with the different Mϕ subsets (GM14, GM16, M14, or M16) at 20:1 T cell/Mϕ ratio for 5 d. Subsequently, lymphocytes were harvested and lymphocyte proliferation was assessed by the CFSE dilution method by flow cytometry.

Cytokine detection in culture supernatants

Mϕs were incubated for 18 h with LPS or left unstimulated. Production of soluble factors in Mϕ SNs was quantified with ELISA kits: IL-1β, TNF, IL-6, IL-23, IL-10 (BD Biosciences), and activin A (R&D Systems).

Western blot

Protein extracts from Mϕ lysates were resolved on reducing 10% polyacrylamide gels and transferred onto polyvinylidene difluoride sheets (Millipore, Bedford, MA). Membranes were incubated with polyclonal Abs to MAFB, PU.1, p50, c-Jun, lamin B (Santa Cruz Biotechnology, Santa Cruz, CA), phospho-Smad2/3, Smad2/3 (Millipore), or mAbs to heme-oxygenase 1 (HO-1; Millipore), RelA, GAPDH, or β-tubulin (Santa Cruz Biotechnology). Then, membranes were incubated with the corresponding HRP-conjugated secondary Abs (Dako, Carpinteria, CA). Bands were detected using ECL (Amersham Biosciences, Piscataway, NJ). Blots were scanned, and densitometric analysis of the autoradiograms was performed with the ImageJ software (version 1.42q).

Microarray analysis

Global gene expression analysis of GM14, M14, GM16, and M16 was performed. RNA was obtained from three independent donors by using the RNeasy Mini kit (Qiagen, Germantown, MD) and analyzed with a whole human genome microarray from Agilent Technologies (Palo Alto, CA). Raw fluorescence data were normalized using the quantiles method as implemented in GeneSpring. For the statistical analysis, only probes with signal values >55% quantile in at least two replicates of at least one out of four conditions evaluated were considered. A mixed lineal model was adjusted to the filtered data using the limma package from the Bioconductor project (http://www.bioconductor.org). Statistical analysis for differential gene expression was carried out by using empirical Bayes moderated *t* test implemented in the limma package. The linear model included two fixed variables (M-Mϕs/GM-Mϕs and CD14^{++}CD16$^-$/CD16$^+$ monocyte-derived Mϕs) and blocking by donor. The *p* values were further adjusted for multiple hypotheses testing using the Benjamini–Hochberg method to control the false discovery rate. Adjusted *p* values <0.05 were considered significant. Except for data normalization, the rest of the procedures were coded in R (http://www.r-project.org). Microarray data are deposited in the Gene Expression Omnibus (http://www.ncbi.nlm.nih.gov/geo/) under accession no. GSE68061.

The differentially expressed genes for all pairs analyzed were assigned to gene ontology (GO) terms by the WebGestalt toolkit (30). Transcription factor (TF) binding site prediction was performed using positional weight matrices from TRANSFAC and JASPAR (http://amp.pharm.mssm.edu/Enrichr). GO terms and TFs were considered significant when they had a Benjamini–Hochberg-corrected *p* value <0.05. For gene set enrichment analysis (GSEA), gene sets containing the top and bottom 150 probes (ranked on the basis of the value of the *t* statistic) from the GM14 versus M14 limma analysis were generated as gene signatures for proinflammatory (GM14) and anti-inflammatory (M14) phenotypes. GSEA analysis for the *t* stastistic–ranked list of genes generated from the M16 versus M14 limma analysis (14,138 genes) was applied on the two gene sets indicated above (31).

Quantitative real-time RT-PCR

Oligonucleotides for selected genes were designed according to the Roche software for RT-quantitative real-time PCR (qRT-PCR). Total RNA was extracted using the RNeasy Mini kit (Qiagen) and retrotranscribed, and individually amplified cDNAs were quantified using the Universal Human Probe Roche library (Roche Diagnostics). Cycling conditions were as follows: 10 min at 95°C, followed by 45 cycles each consisting of 10 s at 95°C and 30 s at 60°C. Assays were made in triplicates and results normalized according to the expression levels of *TBP* mRNA.

Results

Phenotypic and functional features of GM- and M-CSF–derived macrophages

To compare the potential of $CD14^{++}$ $CD16^{-}$ and $CD16^{+}$ human monocyte subpopulations to differentiate along the Mϕ lineage, they were cultured in the continuous presence of either GM-CSF or M-CSF (Fig. 1A). GM-Mϕs had a round-shaped appearance, whereas M-Mϕs displayed spindle morphology (Fig. 1B). The cell yield at the end of the culture was higher in GM14 than in GM16 (Fig. 1C), albeit both monocyte subsets express the GM-CSF receptor (CD116) to a similar extent (Fig. 1D), whereas the cell yield was lower in both M14 and M16 (Fig. 1C). As expected, the four Mϕ populations expressed the lineage-specific marker PU.1 (32) (Fig. 1E), whereas M14 and M16 exhibited higher levels of MAFB and HO-1 (molecules associated with the M-Mϕ phenotype) (32, 33) than did GM14 and GM16 (Fig. 1E). Therefore, both $CD14^{++}$ $CD16^{-}$ and $CD16^{+}$ monocytes differentiate into Mϕs in response to GM-CSF and M-CSF, and they display a profile of myeloid markers that is determined by the priming cytokine.

Subsequently, the phenotypic and the LPS-induced cytokine profiles of the four Mϕ subtypes were assessed. GM14 and GM16 displayed a similar phenotype that concurred with that previously reported (16, 29, 34–36) (Fig. 2A). However, M14 expressed enhanced levels of M-Mϕ–dependent markers (CD14, CD163, CD209, and FRβ) (29) and lower levels of the GM-Mϕ–associated marker CLEC5A (34) than did M16 (Fig. 2A), suggesting a distinct effect of M-CSF on both monocyte subsets. Regarding cytokines, and as expected (13, 15, 29), LPS promoted the release of higher levels of TNF, IL-6, and IL-23, and lower levels of IL-10, in GM-Mϕs compared with M-Mϕs (Fig. 2B). However, LPS-stimulated M16 produced significantly higher amounts of TNF and IL-6 than did M14, whereas IL-10 secretion by M16 was markedly low and comparable to the levels yielded by LPS-treated GM14 or GM16 (Fig. 2B). Additionally, M16 released greater levels of IL-1β than did M14, either constitutively or in response to LPS (Fig. 2C). Therefore, M16 display a more proinflammatory cytokine pattern than do M14. However, both cell subsets showed a similar basal expression and nuclear/cytoplasmic localization of the NF-κB family members p50 and RelA, as well as of the AP-1 family member c-Jun (Fig. 2D, Supplemental Fig. 1). Thus, the distinct LPS-induced cytokine profile of M14 and M16 does not appear to reflect a differential expression of TFs that critically determine Mϕ polarization (37, 38).

Regarding APC ability, both GM14 and GM16 induced the highest rate of lymphocyte proliferation in allogeneic assays, whereas M14 exhibited the weakest APC ability. M16 induced a robust proliferation that was significantly superior with respect to M14 (Fig. 2E). Collectively, these data indicate that GM-CSF

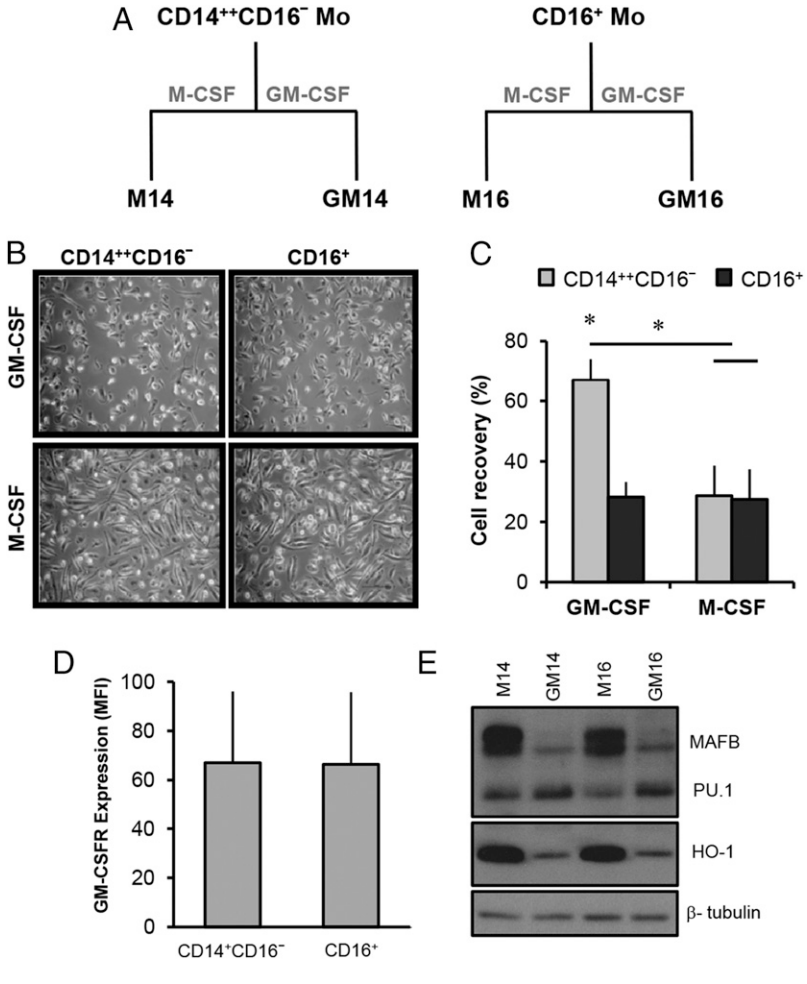

FIGURE 1. Characteristics of $CD14^{++}$ $CD16^{-}$ and $CD16^{+}$ monocyte-derived macrophages. (**A**) Culture conditions for differentiation of human monocyte (Mo)-derived Mϕs. (**B**) Morphology of $CD14^{++}$ $CD16^{-}$ and $CD16^{+}$ monocyte-derived Mϕs after 6 d of culture with GM-CSF (*top panels*) or M-CSF (*bottom panels*). Original magnification ×40. (**C**) Cellular yield of $CD14^{++}$ $CD16^{-}$ and $CD16^{+}$ monocyte-derived Mϕs cultured for 6 d with GM-CSF or M-CSF, expressed as the mean ± SD of five separate donors. (**D**) Expression of CD116 (GM-CSFR) in freshly isolated $CD16^{+}$ and $CD14^{++}CD16^{-}$ human monocytes. All monocytes were $CD116^{+}$. Results are indicated as the mean fluorescence intensity (MFI) of CD116. Shown is the mean ± SD of three independent donors. (**E**) Expression of MAFB, PU.1, and HO-1 by GM16, GM14, M16, and M14. β-Tubulin was used as a loading control. The results are representative of four donors analyzed. Statistical analyses were performed with the paired *t* test. $*p < 0.05$.

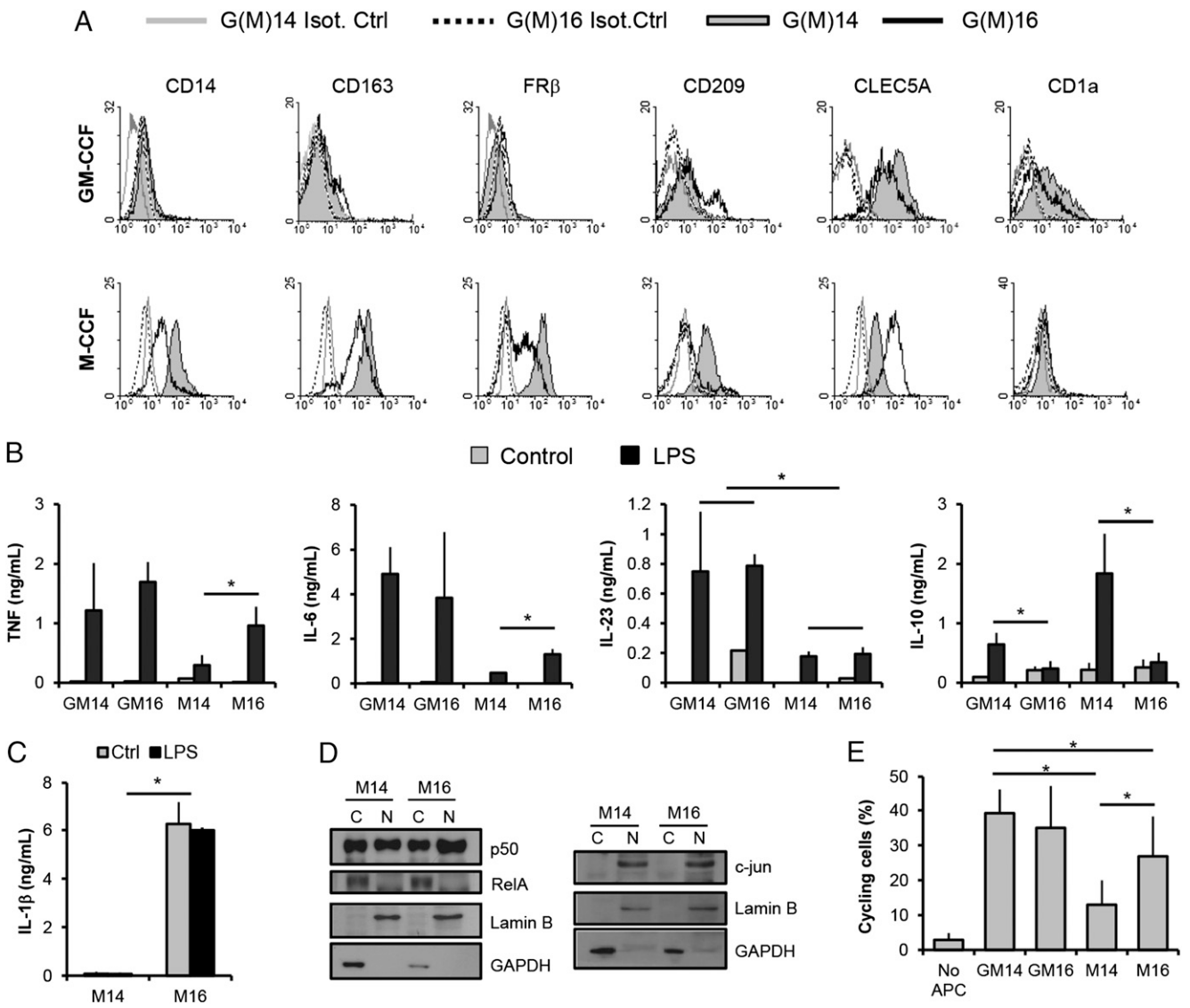

FIGURE 2. Phenotype and functional profile of monocyte-derived macrophages. (**A**) GM14 and M14 (solid gray histograms) and GM16 and M16 (empty black histograms) were assessed for the expression of the indicated markers by flow cytometry. Empty gray and dotted line histograms represent the corresponding Ig isotype-matched controls of G(M)14 and G(M)16, respectively. Results are representative of seven donors evaluated. (**B**) Secretion of TNF, IL-6, IL-23, and IL-10 by GM16, GM14, M16, and M14 in the absence (control) or presence of LPS. (**C**) Production of IL-1β by M14 and M16 in the absence or presence of LPS. (**D**) M14 and M16 from 6-d cultures were directly lysed. Nuclear (N) and cytoplasmic (C) extracts were blotted and probed with Abs against p50, RelA, or c-Jun. Lamin B and GAPDH were used as loading controls for cytoplasm and nucleus, respectively. Shown is the result of a representative experiment out of three to four performed. Densitometric analysis of p50, RelA, and c-Jun bands from the Western blots are depicted in Supplemental Fig. 1. (**E**) Percentage of proliferating allogeneic naive T cells cocultured with GM14, GM16, M14, or M16, or in absence of APC (No APC). In (B), (C), and (E), results are presented as the mean ± SD of three to five independent donors. Statistical analyses were carried out with the paired *t* test. $*p < 0.05$.

promotes a proinflammatory differentiation of both $CD14^{++}$ $CD16^{-}$ and $CD16^{+}$ monocytes, whereas M-CSF exerts a distinct priming effect on both monocyte subpopulations.

M14 and M16 secrete soluble factors that partially dictate their phenotypes

To determine whether soluble factors secreted during the differentiation process influence the distinct phenotype of M14 and M16, conditioned media from M14 and M16 were swapped (Fig. 3A) and the phenotype, cytokine profile, and gene expression of the resulting Mϕs were evaluated. M16 SNs significantly diminished FRβ, CD14, and CD163 expression in M14 and increased their TNF production in response to LPS, although this effect was not statistically significant (Fig. 3B, 3C). Conversely, M14 SNs tended to upregulate FRβ expression, significantly increased CD14 and CD163 expression, reduced the LPS-induced TNF release, and enhanced the LPS-stimulated IL-10 production in M16 (Fig. 3B, 3C). Besides, M14 SNs increased the expression of genes associated with M-CSF–dependent differentiation (*IGF1*, *FOLR2*, *IL10*, and *SERPINB2*) (39) in M16, whereas the opposite occurred in M14 exposed to M16 SNs (Fig. 3D, Table I). Taken together, this set of data confirms that the distinct functional and phenotypic profiles of M14 and M16 are critically determined by factors released by $CD14^{++}$ $CD16^{-}$ and $CD16^{+}$ monocytes upon exposure to M-CSF.

Transcriptomic analysis of the macrophage subsets

To identify the molecular basis for the different properties of M14 and M16, we determined the transcriptional profile of the four Mϕ populations through whole genome microarray assays. Whereas

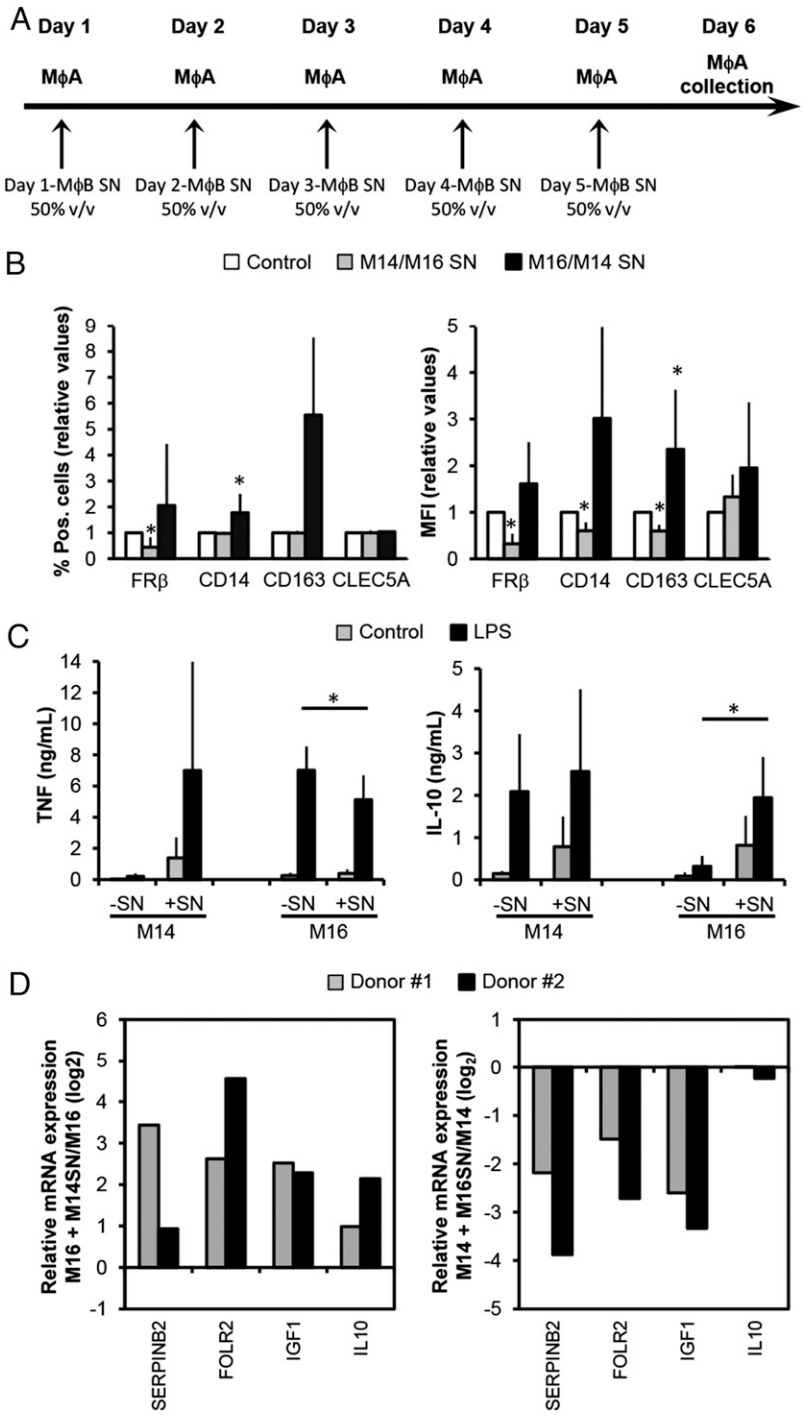

FIGURE 3. M14 and M16 secrete soluble factors that influence their polarization. M14 and M16 were differentiated in the absence or presence of culture SNs from the alternative cell population. (**A**) Scheme of the experimental conditions. Mϕs A and B represent the M14 or M16 subsets. (**B**) Mϕs were harvested after 6 d of culture, and the expression of FRβ, CD14, CD163, and CLEC5A was evaluated by flow cytometry. Shown are the relative percentages of positive cells and the mean fluorescence intensity (MFI) for each marker in control Mϕs (white bars), in M14 differentiated with M16 SNs (gray bars), and in M16 cultured with M14 SNs (black bars). The results depicted are the mean ± SD of six donors evaluated. (**C**) Secretion of TNF and IL-10 by M16 and M14 stimulated with LPS and in unstimulated (control) cells. M14 and M16 were cultured in the absence (−SN) or presence (+SN) of culture SNs from the alternative cell population. Shown is the mean ± SD of three to four independent donors. (**D**) Relative expression ($\log_2$) of the indicated M-Mϕ–related genes in M14 and M16 cultured as in (A), determined by qRT-PCR in two separate donors. Shown is the relative gene expression (relative to *TBP* mRNA levels) in M16 cultured with M14 SNs with respect to the expression in M16 (*left panel*) and in M14 cultured with M16 SNs referred to the expression in M14 (*right panel*). Statistical analyses were performed with the paired *t* test. $^*p < 0.05$.

1569 genes were differentially (≥2-fold change, adjusted p value < 0.05) expressed between GM14 and M14 (916 genes preferentially expressed in GM14, 653 in M14), only 517 genes showed a distinct expression between GM16 and M16 (382 genes with higher expression in M16, 135 in GM16) (Fig. 4A, Supplemental Table I), thus reflecting that the transcriptional profiles of GM16 and M16 are more similar to each other than those of GM14 and M14. Of note, 81% of the genes overexpressed in GM16 with respect to M16 were also overexpressed in GM14 with respect to M14, but only 49% of the genes overexpressed in M16 when compared with GM16 were also significantly overexpressed in M14 relative to GM14. Moreover, unsupervised hierarchical clustering using the expression of the 80 most differentially expressed genes between GM-Mϕs and M-Mϕs reflected that GM14 and GM16 are most closely related to each other, whereas M14 and M16 were more distantly clustered (Supplemental Fig. 2).

The differentially expressed genes were analyzed for GO biological process and TF enrichment. All gene sets were significantly associated to "immune system" and "response to stimuli" processes, and most of them were also associated with "cell proliferation" and "apoptosis" terms (Supplemental Table II). GM14- and M14-overexpressed genes were significantly enriched in "response to wounding" process, and GO terms particularly associated with M14-enriched genes were related to "system developmental processes," "response to lipids," and "chemotaxis". Notably, genes with preferential expression in GM-Mϕs were significantly associated with "response to type I interferon." Pathways associated to "nucleosome organization" were over-

Table I. Sequences of the oligonucleotides used for qRT-PCR

Gene	Forward Primer (5′→3′)	Reverse Primer (5′→3′)
CCR2B	TGAGACAAGCCACAAGCTGA	TTCTGATAAACCGAGAACGAGAT
ECSCR	AGCTGTGCTGGGTGATCCT	ATTGTGGGCTGGGAGTTGT
EGLN3	ATCGACAGGCTGGTCCTCTA	GATAGCAAGCCACCATTG C
FOLR2	GAGAGAGGCCAACTCAGACAC	CCAGACCATGTCTTTCTGTCC
IGF1	TGTGGAGACAGGGGCTTTTA	ATCCACGATGCCTGTCTGA
IL1B	CTGTCCTGCGTGTTGAAAGA	TTGGGTAATTTTTGGGATCTACA
IL10	GTGGAGCAGGTGAAGAATGC	TCACTCATGGCTTTGTAGATGC
INHBA	CTCGGAGATCATCACGTTTG	CCTTGGAAATCTCGAAGTGC
SERPINB2	CATGGAGCATCTCGTCCAC	ACTGCATTGGCTCCCACTT
SERPINE1	AAGGCACCTCTGAGAACTTCA	CCCAGGACTAGGCAGGTG
TBP	CGGCTGTTTAACTTCGCTTC	CACACGCCAAGAAACAGTGA

represented in GM16 and, remarkably, genes overexpressed in M16 were found to be associated with several processes related with cell cycle (Supplemental Table II). Regarding TFs, the genes upregulated in both GM14 and M14 were enriched in targets of TFs such as c-Fos and C/EBP-β. Targets of Smad4, STAT1, or c-Jun were enriched within the list of genes with higher expression in GM14 (relative to M14), whereas targets of STAT3, peroxisome proliferator–activated receptor (PPAR)-γ, CREB, or Gli2 appeared enriched within the genes overrepresented in M14 (relative to GM14). Genes overexpressed in both GM16 and M16 were enriched in targets of a common set of TFs and transcriptional regulators such as Smad4, C/EBP-α, IFN regulatory factor (IRF)-8, recombination signal binding protein for Igκ J region, or PPAR-γ. The genes overexpressed in GM16 (relative to M16) were enriched in Sp-1 and Sp-3, Kruppel-like factor-4, -5, and -11, or Snail1 and 2 targets, whereas targets of STAT1, STAT3, AP-1 (c-Fos, c-Jun, JunD), and C/EBP-β and -ε were predicted to be enriched in M16-overrepresented genes (Supplemental Table III). The upregulated genes in the four Mϕ subpopulations were enriched in NF-κB (p50, RelA) targets, suggesting that these TFs might have a role in the function/development of the Mϕ lineage.

The M16 gene expression signature is skewed toward the proinflammatory side and resembles that of macrophages differentiated in the presence of GM-CSF

A further comparison was performed between the gene expression profiles of GM16 and GM14 and between those of M16 and M14 (Fig. 4A, Supplemental Table I). One hundred ninety-eight genes were differentially expressed between GM14 and GM16 (21 upregulated and 177 downregulated in GM16 compared with GM14), whereas only 68 genes were differentially expressed between M14 and M16 (41 upregulated and 27 downregulated in M16 compared with M14). GO terms significantly associated with GM14 upregulated genes were all related with cell cycle, which concurred with the enrichment of TF targets involved in cell cycle regulation within GM14 overrepresented genes. Few GO annotations and no TFs were significantly enriched in the set of genes differentially expressed in M16 versus M14 (Supplemental Tables II, III).

Unsupervised hierarchical clustering of the genes differentially expressed between M14 and M16 revealed that the gene expression pattern of M16 was more closely related to those of GM-Mϕs than to the M14 (Fig. 4B). The GM-Mϕ trademark of the M16 transcriptome was further confirmed by analyzing the expression of representative GM-CSF–dependent (*EGLN3*, *ECSCR*, *CCR2*, *IL1B*, and *INHBA*) and M-CSF–dependent (*IL10*, *IGF1*, *FOLR2*, and *SERPINB2*) (39–41) genes (Table I, Supplemental Fig. 3). Moreover, when the ranked list of genes generated from the M16 versus M14 limma analysis (14,138 genes) was subjected to GSEA for statistical associations with pro- and anti-inflammatory gene signatures (derived from the GM14 versus M14 comparison, as indicated in *Materials and Methods*), the proinflammatory signature was significantly enriched in M16 overrepresented genes (Fig. 4C, *upper panel*), whereas the anti-inflammatory signature was associated with M14 overexpressed genes (Fig. 4C, *lower panel*). Taken together, these data indicate that M16 exhibit a gene expression signature that is more closely related to that of proinflammatory GM-Mϕs than to the anti-inflammatory signature of M14.

M16-derived activin A impairs the acquisition of anti-inflammatory traits

Because activin A contributes to the acquisition of the GM-CSF–dependent gene profile (39, 42), we tested whether activin A could account for the distinct transcriptional signatures of M16 and M14. M16 constitutively produced larger amounts of activin A than did M14 (Fig. 5A) and exhibited higher levels of phosphorylated Smad2/3 (Fig. 5B, Supplemental Fig. 1). Activin A secretion by M16 was partially dependent on IL-6 and, predominantly, on TNF released by CD16$^+$ monocytes during their culture with M-CSF, but it did not seem to be an intrinsic property of this monocyte subset because the levels of *INHBA* transcripts were analogous in CD16$^+$ and CD14^{++}CD16$^-$ monocytes (Supplemental Fig. 4). Importantly, blockade of activin A receptors with the inhibitor A83-01 along the M16 differentiation process resulted in increased expression of M-CSF–associated genes (*SERPINB2* and *FOLR2*) and cell surface molecules (FRβ, CD14, and CD163), as well as in reduced expression of GM-CSF–associated genes (*SERPINE1* and *EGLN3*) and of the GM-CSF–inducible marker CLEC5A (Fig. 5C, 5D, Table I). Moreover, most of the transcriptional and phenotypic effects of M16-conditioned media on M14 were reverted by blocking activin A receptors (Fig. 5E, 5F). At the functional level, the presence of A83-01 slightly diminished the LPS-induced IL-10 secretion by M16 and had no effect on TNF production (Fig. 5G). In agreement with the data depicted in Fig. 3C, activin A from M16 SNs did not seem to be connected with the production of TNF or IL-10 by LPS-stimulated M14 (Fig. 5H). Collectively, these data demonstrate that activin A partially accounts for the distinct transcriptional and phenotypic properties of M16 and M14, and that the release of activin A from differentiating CD16$^+$ monocytes contributes to the proinflammatory profile of M16.

M14-derived IL-10 strongly conditions the acquisition of an M-CSF–dependent anti-inflammatory profile

Finally, we assessed whether M14-derived soluble factors also contribute to the distinct profiles of M14 and M16 through neutralizing experiments. We found that IL-10 neutralization along the M14 differentiation process led to reduced expression of FRβ,

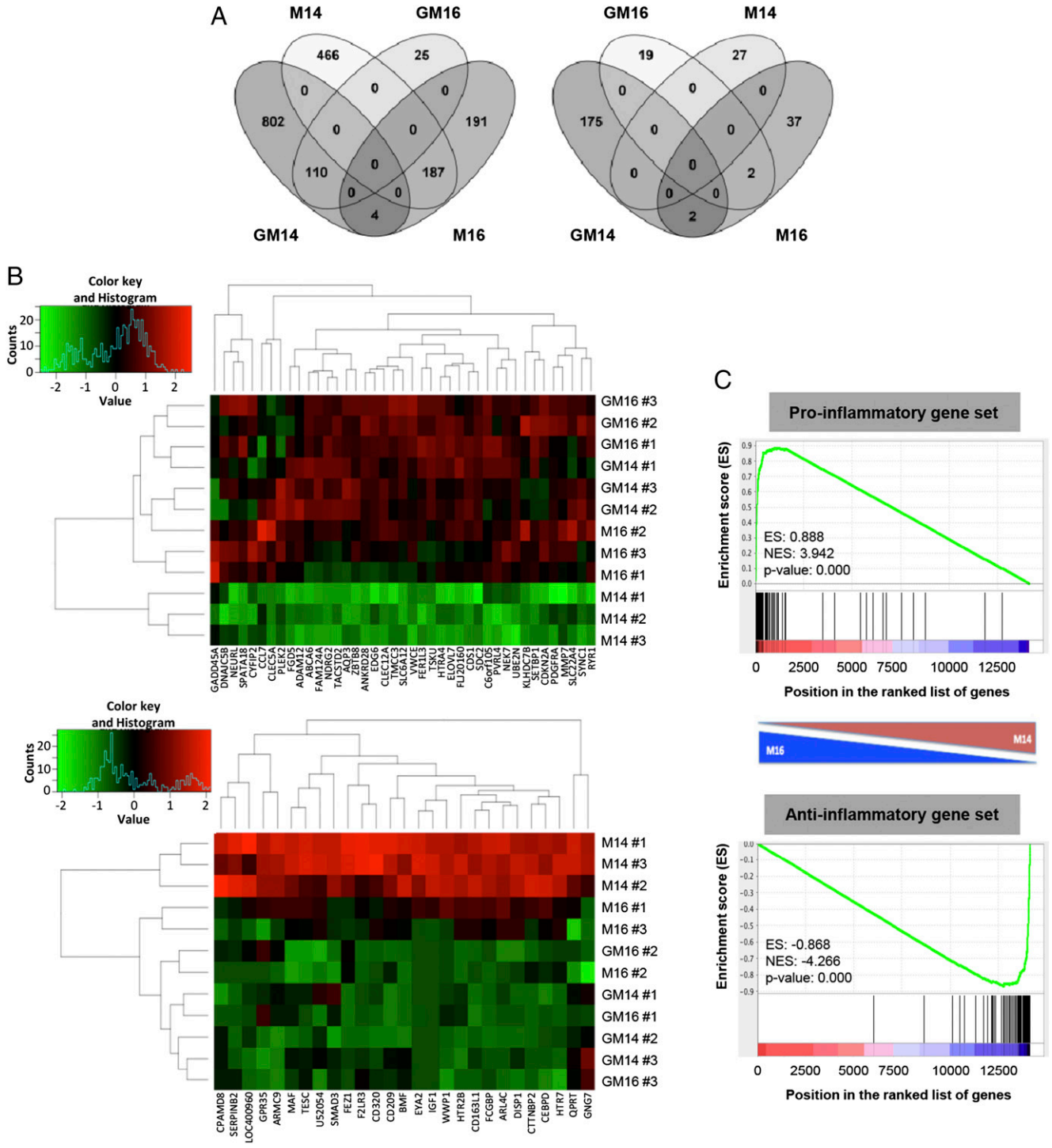

FIGURE 4. Differentially expressed genes in the macrophage subpopulations by microarray assays. (**A**) Venn diagrams of statistically significant changes of gene expression in GM14, GM16, M14, and M16. Shown are the comparisons of GM14 versus M14 and GM16 versus M16 (*left*) and GM16 versus GM14 and M16 versus M14 (*right*). (**B**) Heat maps representing color-coded relative normalized expression levels of the genes differentially expressed between M16 and M14 from biological donors 1–3 used for the microarray experiments. *Upper panel*, upregulated genes found in M16 with respect to M14; *lower panel*, upregulated genes found in M14 with respect to M16. (**C**) GSEA analysis of the *t* stastistic–ranked list of genes obtained from the M16 versus M14 limma analysis, using the proinflammatory (*upper panel*) and anti-inflammatory (*lower panel*) gene sets generated as described in *Materials and Methods*. For comparative purposes, a diagram illustrating the relative expression of the genes in the ranked list in both Mϕ subtypes (M16 and M14) is shown between both panels. ES, enrichment score; NES, normalized enrichment score.

CD14, and CD163, and to enhanced CLEC5A levels (Fig. 6A). Moreover, IL-10 blockade reversed 1) the ability of M14 SNs to augment FRβ, CD14, and CD163 cell surface expression in M16 (Fig. 6B), and 2) the transcriptional effect of M14 SNs on the expression of M-CSF–associated (*FOLR2*, *SERPINB2*, *IGF1*, and *IL10*) and GM-CSF–associated genes (*SERPINE1* and *EGLN3*) in M16 (Fig. 6C). Along this line, swapping of conditioned media revealed that the reduced TNF secretion of M16 cultured with M14 SNs was reverted when IL-10 was blocked, although this effect was not statistically significant (Fig. 6D, *left panel*). Lastly,

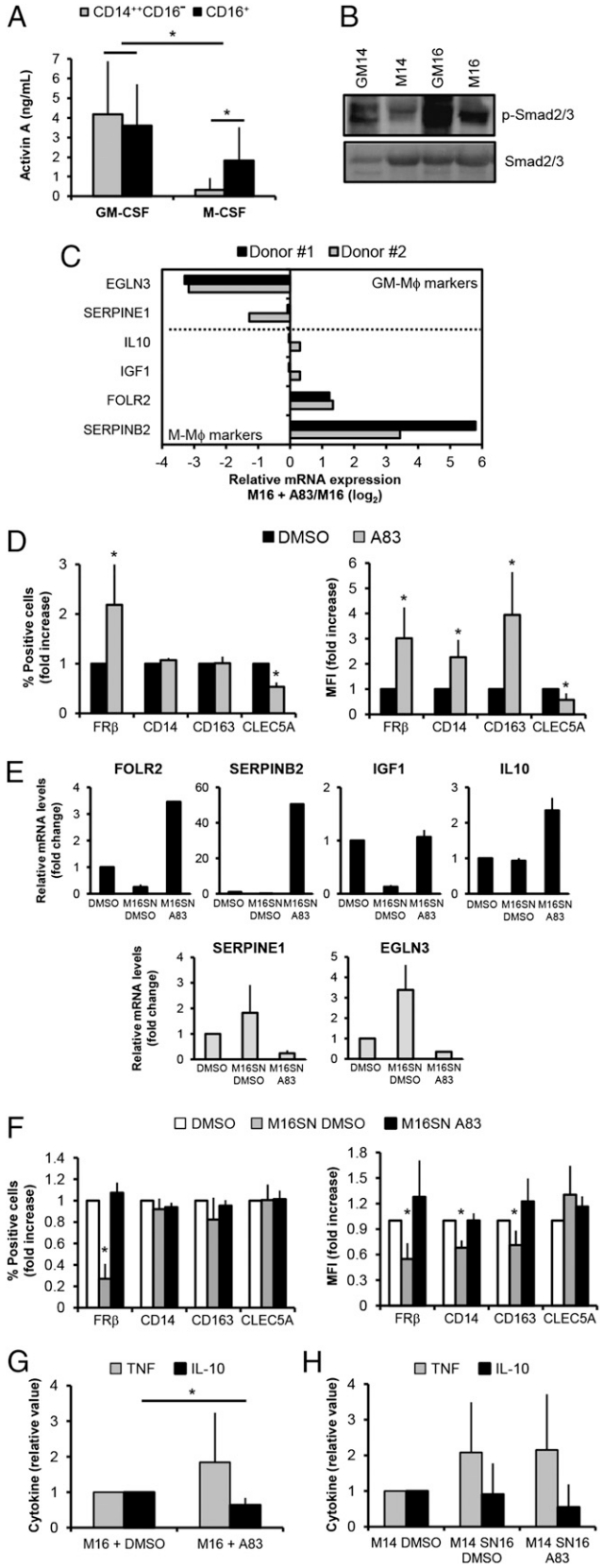

FIGURE 5. M16 produce high levels of activin A. (**A**) Activin A levels in 6-d culture SNs from GM14, GM16, M14, and M16, detected by ELISA. The data are the means ± SD of seven independent donors. (**B**) Smad2/3 expression and activation (p-Smad2/3) in GM14, GM16, M14, and M16 differentiated for 6 d. Shown is the result of a representative experiment out of four performed. Densitometric analysis of p-Smad2/3 and Smad2/3 bands from the Western blots is presented in Supplemental Fig. 1. (**C**) Relative expression (log_2) of GM- and M-Mϕ–related genes (relative to *TBP* mRNA levels) determined by qRT-PCR in M16 differentiated in the presence of A83-01 (A83) or DMSO (vehicle). Results shown are the expression of each gene in A83-01–treated Mϕs referred to its expression in DMSO-treated Mϕs in two different donors. (**D**) Phenotype of M16 generated as in (C). Shown is the expression of the indicated markers (percentage of positive cells and mean fluorescence intensity [MFI]) in A83-01–treated Mϕs (A83) relative to DMSO-treated Mϕs, and results are the means ± SD of four independent donors. (**E**) Relative expression of M-Mϕ– (*top*) and GM-Mϕ–associated (*bottom*) genes (relative to *TBP* mRNA levels) determined by qRT-PCR in M14 differentiated in the absence (DMSO) or presence of M16 culture SNs plus DMSO (M16SN DMSO) or plus A83-01 (M16SN A83). Values are depicted as the fold change with respect to the DMSO condition. Graphs represent the mean ± SD of two different experiments. (**F**) Phenotype of M14 generated as in (E). The percentages of positive cells and the MFI for each marker relative to control Mϕs (DMSO, white bars) in M14 differentiated with M16 SNs in the presence of DMSO (gray bars) and in M14 cultured with M16 SNs in the presence of A83-01 (black bars) are depicted. The results are the means ± SD of three donors evaluated. (**G**) Production of TNF and IL-10 in response to LPS by A83-01–treated M16 (M16 + A83) relative to DMSO-treated cells (M16 + DMSO), represented as the means ± SD of five separate donors. (**H**) TNF and IL-10 secretion by LPS-stimulated M14 generated as in (E). Shown are the values obtained relative to the condition with DMSO, represented as the mean ± SD of three independent donors. Statistical analyses were performed with the paired *t* test. $*p < 0.05$.

and as expected, IL-10 blockade during M14 cultures led to a pronounced increase in the LPS-stimulated production of TNF (Fig. 6D, *right panel*). Therefore, the constitutive release of IL-10 notably promotes the acquisition of the M14 polarization profile, whereas the lack of IL-10 production contributes to the proinflammatory phenotypic, transcriptomic, and functional profile of M16.

Discussion

Mϕs are highly plastic cells that adapt their phenotype and functions according to the surrounding microenvironment. In this study, we report that a subtype of human blood monocytes, namely CD16+ monocytes, have a restricted potential of differentiation toward the anti-inflammatory Mϕ phenotype. We found that whereas the more immature $CD14^{++}CD16^{-}$ monocyte subset is able to acquire pro- and anti-inflammatory properties when cultured with GM-CSF or M-CSF, respectively, the intermediate/nonclassical CD16+ monocytes fail to differentiate into anti-inflammatory Mϕs in the presence of M-CSF. Their high secretion of activin A and the lack of IL-10 production contribute to this limitation.

The inflammatory traits of CD16+ monocytes have been documented (2, 6–8, 10). MAPK and NF-κB strongly mediate the production of proinflammatory cytokines by CD16+ monocytes (6, 43), although the molecular basis of their inability to produce IL-10 are currently unknown. The proinflammatory nature of CD16+ monocytes was confirmed in the M-CSF–differentiating system, where they release high amounts of activin A in the absence of LPS by virtue of their early secretion of TNF and IL-6. Moreover, regarding fully differentiated Mϕs, LPS-stimulated M16 produce high levels of TNF and low amounts of IL-10, whereas M14 act inversely. This behavior is not associated to a distinct basal expression or cellular localization of p50, p65, and c-Jun, although we cannot discount that the activity of these TFs will be differentially modified in LPS-activated M16 and M14.

Besides the proinflammatory cytokine pattern of M16, they share several characteristics with GM-Mϕs at the phenotypic, functional,

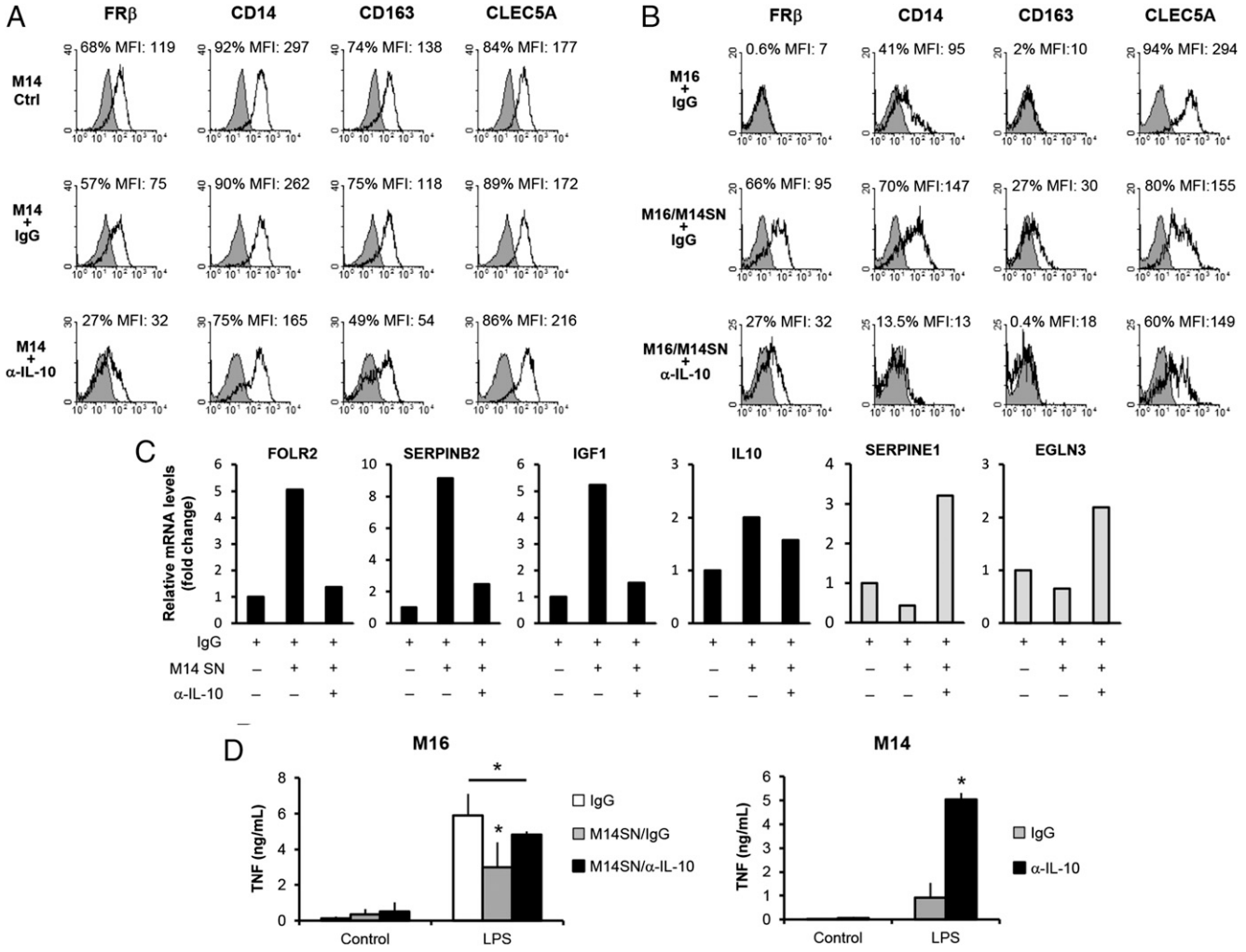

FIGURE 6. M14 produce IL-10 that favors the acquisition of M-CSF polarization markers in M16. (**A**) M14 were cultured in the absence of treatment (Ctrl), with control Ig (M14 + IgG), or with a neutralizing mAb to IL-10 (M14 + α-IL-10). (**B**) M16 were differentiated in the absence or presence of M14 culture SNs (M14SN) and treated with a blocking mAb to IL-10 (α-IL10) or control Ig (IgG). After 6 d, the expression of FRβ, CD14, CD163, and CLEC5A (open histograms) was evaluated by flow cytometry in M14 (A) and M16 (B). Gray-filled histograms correspond to the staining of isotype-matched control Abs. The percentage of positive cells and the mean fluorescence intensity (MFI) for each marker are indicated at the top of the histograms. Data shown are from a representative donor out of two analyzed. (**C**) Relative expression of M- (black bars) and GM-Mϕ–related (gray bars) genes in M16 generated as in (B), determined by qRT-PCR (relative to *TBP* mRNA levels). Results are shown as the expression of each gene in M16 differentiated with M14 SNs (grown with control Ig [IgG] or a blocking mAb to IL-10 [α-IL-10]) referred to its expression with IgG in the absence of M14 SNs. (**D**) Production of TNF by M16 (*left*) or M14 (*right*) treated as in (A) (M14) or (B) (M16) and stimulated with LPS or left unstimulated (Control). Graphs illustrate the mean ± SD of three independent donors. Statistical analyses were performed with the paired *t* test. $*p < 0.05$.

and transcriptomic level. In a previous study, Frankenberger et al. (44) reported that M16 expressed a lower level of CD14 and CD163 transcripts with respect to M14. In the present study, we corroborate that the expression of key phenotypic markers of M-Mϕs (CD14, CD163, CD209, and FRβ) (29) is greatly diminished in M16, whereas they abundantly express the GM-CSF–associated marker CLEC5A (34). Additionally, M16 display an enhanced APC ability compared with M14, which is characteristic of GM-Mϕs (13, 15). Lastly, gene clustering and GSEA analyses show that GM-Mϕs and M16 are closely related whereas M14 are more separately clustered, and that M16 gene expression is strongly associated with a proinflammatory signature. Because activin A highly contributes to the GM-Mϕ gene expression pattern (39, 42), it is likely that the similarity of the GM-Mϕ and M16 transcriptomes was partially owed to the constitutive production of this cytokine by these cell subsets. The lack of IL-10 production by M16 might act in concert with activin A to support that similitude (42). Overall, these are intriguing findings because M-CSF–driven differentiation leads to the acquisition of M2-polarizing attributes in total $CD14^+$ monocytes (45), and the transcriptomic profile of M-Mϕs is much closer to that of IL-4–primed (M2) than to that of LPS/IFN-γ–primed (M1) Mϕs (46). The proinflammatory skewing of M-CSF−cultured $CD16^+$ monocytes could rely on their more mature status compared with classical $CD14^{++}CD16^-$ monocytes (4, 5), which may restrict their potential for differentiation. Additionally, the proinflammatory signature of $CD16^+$ monocytes might impair their full reprogramming toward the M2 side of the activation spectrum.

Our work provides some insights into the functions and molecular pathways that could be associated with pro- and anti-inflammatory monocyte differentiation. Overall, the GO pathways related to GM14 and M14, the most extremely polarized cells, are in agreement with those previously reported (42). The enrichment of the "response to type I interferon" pathway in GM-Mϕs versus M-Mϕs suggests that, contrary to that reported in mice (47), endogenously produced type I IFN might have more relevant roles in the former

cells. GO analysis also suggests that processes related with cell cycle are significantly suppressed in GM16, because they are enriched in M16 and GM14 relative to GM16 genes, and this could explain the low cell yield of the GM16 subset.

Several TFs have been associated to the M1/M2 Mϕ differentiation. Mediators of M1 polarization include NF-κB p50–p65 heterodimers, AP-1, STAT1, C/EBP-α, and IRF-3, -5, -8, and -9, whereas M2 polarization–promoting TFs include NF-κB p50–p50 homodimers, STAT3, STAT6, C/EBP-β, Krüppel-like factor-4, or PPAR-γ (37, 48, 49). Corroborating the dual role of NF-κB, we found that these TFs could be involved in the function or development of the pro- and the anti-inflammatory phenotypes in the GM-CSF/M-CSF system. STAT3, a key transcription regulator of IL-10 and IL-6, was found strongly associated with M-Mϕs, whereas Smad4, AP-1, and STAT1 were predicted to be enriched in the cells with a proinflammatory skew, that is, GM-Mϕs and M16. Of note, the overrepresentation of Smad4 target genes in these Mϕ subsets parallels their activin A release. GM16 and M16 also shared predicted TFs and transcriptional regulators associated with the M1 phenotype, such as C/EBP-α, IRF-8, and recombination signal binding protein for Igκ J region (49). Therefore, the analysis of TF binding sites in M16 overrepresented genes reinforces their proinflammatory nature and provides additional tools to elucidate the molecular pathways involved in their differentiation.

The role of the mouse orthologous Ly6C^{hi} (CD14^{++}CD16$^-$) and Ly6C^{lo} (CD16$^+$) monocyte subsets in diverse experimental pathological settings remains unclear. Some studies have reflected the anti-inflammatory, proangiogenic, and tissue repair functions of Ly6C^{lo} monocytes (20, 24). However, these cells could derive from the infiltrating, inflammatory Ly6C^{hi} monocytes that downregulate Ly6C surface expression upon tissue arrival (23). Thus, Ly6C^{hi} monocytes are recruited to inflamed tissues where they could develop proinflammatory activities (22, 24). Subsequently, the accumulation of cell debris from dead neutrophils and tissue cells may trigger Ly6C^{hi} monocyte repolarization toward an anti-inflammatory/proresolution phenotype that facilitates tissue regeneration (23, 27, 50, 51). These findings are consistent with the high plasticity of conventional human CD14^{++}CD16$^-$ monocytes (2) that can develop an M1-like profile in proinflammatory environments (GM-CSF), but can also acquire proresolution phenotypes in tissue repair scenarios (M-CSF). It has been proposed that Ly6C^{lo} monocytes are terminally differentiated blood-resident Mϕs with a role in the maintenance of vessel integrity by their ability to interact with the vascular endothelia and to scavenge particles at the luminal side of capillaries (52). Whether this applies for human CD16$^+$ monocytes is uncertain. It has been shown that nonclassical CD14$^+$CD16^{++} monocytes attached to and crawled on vessel endothelia after i.v. transfer into *Rag2*$^{-/-}$ *Il2rg*$^{-/-}$ *Cx3cr1*^{gfp} mice, whereas attachment was not observed after classical CD14^{++}CD16$^-$ or intermediate CD14^{++}CD16$^+$ monocyte transfer (6), suggesting that nonclassical human monocytes could have a role in blood vessel homeostasis. However, these cells display low phagocytic ability (6, 53), which is opposed to what was found for their Ly6C^{lo} murine counterpart. Thus, human and murine nonclassical monocyte subsets are not fully analogous and it is difficult to infer a role for CD16$^+$ cells. Our results imply that M-CSF, which is constitutively present in the blood at high levels (54), is not only a differentiating cytokine for CD16$^+$ monocytes (4) but also drives their proinflammatory priming, which is mainly supported by activin A. Because several studies have attributed a role of this cytokine in neovascularization and vascular remodeling (55, 56), it is plausible that CD16$^+$ monocytes would have a role in blood vessel homeostasis through activin A secretion, although an effect of this cytokine has not been demonstrated in Ly6C^{lo} mouse monocytes.

In summary, our results suggest that the CD16$^+$ monocyte subset has a certain degree of commitment to become Mϕs with unique specific functions. Whereas CD14^{++}CD16$^-$ monocytes exhibit high plasticity and are precursors of pro- and anti-inflammatory Mϕs, CD16$^+$ monocytes are more prone to generate Mϕs with a proinflammatory shift. The constitutive release of activin A and the lack of IL-10 favor the proinflammatory skewing of CD16$^+$ monocyte-derived Mϕs when they are generated in an anti-inflammatory environment dictated by M-CSF. However, these Mϕs are able to repolarize to some extent when they developed in anti-inflammatory milieus containing IL-10. Therefore, CD16$^+$ monocyte–derived Mϕs would only acquire anti-inflammatory/proresolution phenotypes within specific tissue environments.

Acknowledgments

We gratefully acknowledge Enrique Sánchez-Torres for critical reading of the manuscript and offering comments that improved its contents. We also thank Víctor H. Rosales for help with flow cytometry, Dr. T. Matsuyama for the Ab against FRβ, Julio C. Ramírez for technical assistance, and Ninfa Arreola for aid in the preparation of the manuscript (Centro de Investigación y de Estudios Avanzados del Instituto Politécnico Nacional).

Disclosures

The authors have no financial conflicts of interest.

References

1. Serbina, N. V., T. Jia, T. M. Hohl, and E. G. Pamer. 2008. Monocyte-mediated defense against microbial pathogens. *Annu. Rev. Immunol.* 26: 421–452.
2. Wong, K. L., J. J. Tai, W. C. Wong, H. Han, X. Sem, W. H. Yeap, P. Kourilsky, and S. C. Wong. 2011. Gene expression profiling reveals the defining features of the classical, intermediate, and nonclassical human monocyte subsets. *Blood* 118: e16–e31.
3. Ziegler-Heitbrock, L., P. Ancuta, S. Crowe, M. Dalod, V. Grau, D. N. Hart, P. J. Leenen, Y. J. Liu, G. MacPherson, G. J. Randolph, et al. 2010. Nomenclature of monocytes and dendritic cells in blood. *Blood* 116: e74–e80.
4. Korkosz, M., K. Bukowska-Strakova, S. Sadis, T. Grodzicki, and M. Siedlar. 2012. Monoclonal antibodies against macrophage colony-stimulating factor diminish the number of circulating intermediate and nonclassical (CD14^{++}CD16$^+$/CD14$^+$CD16^{++}) monocytes in rheumatoid arthritis patient. *Blood* 119: 5329–5330.
5. Weiner, L. M., W. Li, M. Holmes, R. B. Catalano, M. Dovnarsky, K. Padavic, and R. K. Alpaugh. 1994. Phase I trial of recombinant macrophage colony-stimulating factor and recombinant γ-interferon: toxicity, monocytosis, and clinical effects. *Cancer Res.* 54: 4084–4090.
6. Cros, J., N. Cagnard, K. Woollard, N. Patey, S. Y. Zhang, B. Senechal, A. Puel, S. K. Biswas, D. Moshous, C. Picard, et al. 2010. Human CD14^{dim} monocytes patrol and sense nucleic acids and viruses via TLR7 and TLR8 receptors. *Immunity* 33: 375–386.
7. Belge, K. U., F. Dayyani, A. Horelt, M. Siedlar, M. Frankenberger, B. Frankenberger, T. Espevik, and L. Ziegler-Heitbrock. 2002. The proinflammatory CD14$^+$CD16$^+$DR^{++} monocytes are a major source of TNF. *J. Immunol.* 168: 3536–3542.
8. Mizuno, K., T. Toma, H. Tsukiji, H. Okamoto, H. Yamazaki, K. Ohta, K. Ohta, Y. Kasahara, S. Koizumi, and A. Yachie. 2005. Selective expansion of CD16^{high} CCR2$^-$ subpopulation of circulating monocytes with preferential production of haem oxygenase (HO)-1 in response to acute inflammation. *Clin. Exp. Immunol.* 142: 461–470.
9. Ziegler-Heitbrock, H. W. 1996. Heterogeneity of human blood monocytes: the CD14$^+$ CD16$^+$ subpopulation. *Immunol. Today* 17: 424–428.
10. Frankenberger, M., T. Sternsdorf, H. Pechumer, A. Pforte, and H. W. Ziegler-Heitbrock. 1996. Differential cytokine expression in human blood monocyte subpopulations: a polymerase chain reaction analysis. *Blood* 87: 373–377.
11. Ziegler-Heitbrock, L. 2007. The CD14$^+$ CD16$^+$ blood monocytes: their role in infection and inflammation. *J. Leukoc. Biol.* 81: 584–592.
12. Locati, M., A. Mantovani, and A. Sica. 2013. Macrophage activation and polarization as an adaptive component of innate immunity. *Adv. Immunol.* 120: 163–184.
13. Fleetwood, A. J., T. Lawrence, J. A. Hamilton, and A. D. Cook. 2007. Granulocyte-macrophage colony-stimulating factor (CSF) and macrophage CSF-dependent macrophage phenotypes display differences in cytokine profiles and transcription factor activities: implications for CSF blockade in inflammation. *J. Immunol.* 178: 5245–5252.

14. Biswas, S. K., A. Sica, and C. E. Lewis. 2008. Plasticity of macrophage function during tumor progression: regulation by distinct molecular mechanisms. *J. Immunol.* 180: 2011–2017.
15. Verreck, F. A., T. de Boer, D. M. Langenberg, M. A. Hoeve, M. Kramer, E. Vaisberg, R. Kastelein, A. Kolk, R. de Waal-Malefyt, and T. H. Ottenhoff. 2004. Human IL-23-producing type 1 macrophages promote but IL-10-producing type 2 macrophages subvert immunity to (myco)bacteria. *Proc. Natl. Acad. Sci. USA* 101: 4560–4565.
16. Puig-Kröger, A., E. Sierra-Filardi, A. Domínguez-Soto, R. Samaniego, M. T. Corcuera, F. Gómez-Aguado, M. Ratnam, P. Sánchez-Mateos, and A. L. Corbí. 2009. Folate receptor β is expressed by tumor-associated macrophages and constitutes a marker for M2 anti-inflammatory/regulatory macrophages. *Cancer Res.* 69: 9395–9403.
17. Geissmann, F., S. Jung, and D. R. Littman. 2003. Blood monocytes consist of two principal subsets with distinct migratory properties. *Immunity* 19: 71–82.
18. Tacke, F., and G. J. Randolph. 2006. Migratory fate and differentiation of blood monocyte subsets. *Immunobiology* 211: 609–618.
19. Ingersoll, M. A., R. Spanbroek, C. Lottaz, E. L. Gautier, M. Frankenberger, R. Hoffmann, R. Lang, M. Haniffa, M. Collin, F. Tacke, et al. 2010. Comparison of gene expression profiles between human and mouse monocyte subsets. *Blood* 115: e10–e19.
20. Auffray, C., D. Fogg, M. Garfa, G. Elain, O. Join-Lambert, S. Kayal, S. Sarnacki, A. Cumano, G. Lauvau, and F. Geissmann. 2007. Monitoring of blood vessels and tissues by a population of monocytes with patrolling behavior. *Science* 317: 666–670.
21. Misharin, A. V., C. M. Cuda, R. Saber, J. D. Turner, A. K. Gierut, G. K. Haines, III, S. Berdnikovs, A. Filer, A. R. Clark, C. D. Buckley, et al. 2014. Nonclassical Ly6C$^-$ monocytes drive the development of inflammatory arthritis in mice. *Cell Reports* 9: 591–604.
22. Karlmark, K. R., R. Weiskirchen, H. W. Zimmermann, N. Gassler, F. Ginhoux, C. Weber, M. Merad, T. Luedde, C. Trautwein, and F. Tacke. 2009. Hepatic recruitment of the inflammatory Gr1$^+$ monocyte subset upon liver injury promotes hepatic fibrosis. *Hepatology* 50: 261–274.
23. Dal-Secco, D., J. Wang, Z. Zeng, E. Kolaczkowska, C. H. Wong, B. Petri, R. M. Ransohoff, I. F. Charo, C. N. Jenne, and P. Kubes. 2015. A dynamic spectrum of monocytes arising from the in situ reprogramming of CCR2$^+$ monocytes at a site of sterile injury. *J. Exp. Med.* 212: 447–456.
24. Nahrendorf, M., F. K. Swirski, E. Aikawa, L. Stangenberg, T. Wurdinger, J. L. Figueiredo, P. Libby, R. Weissleder, and M. J. Pittet. 2007. The healing myocardium sequentially mobilizes two monocyte subsets with divergent and complementary functions. *J. Exp. Med.* 204: 3037–3047.
25. Shechter, R., O. Miller, G. Yovel, N. Rosenzweig, A. London, J. Ruckh, K. W. Kim, E. Klein, V. Kalchenko, P. Bendel, et al. 2013. Recruitment of beneficial M2 macrophages to injured spinal cord is orchestrated by remote brain choroid plexus. *Immunity* 38: 555–569.
26. Dunay, I. R., R. A. Damatta, B. Fux, R. Presti, S. Greco, M. Colonna, and L. D. Sibley. 2008. Gr1$^+$ inflammatory monocytes are required for mucosal resistance to the pathogen *Toxoplasma gondii*. *Immunity* 29: 306–317.
27. Egawa, M., K. Mukai, S. Yoshikawa, M. Iki, N. Mukaida, Y. Kawano, Y. Minegishi, and H. Karasuyama. 2013. Inflammatory monocytes recruited to allergic skin acquire an anti-inflammatory M2 phenotype via basophil-derived interleukin-4. *Immunity* 38: 570–580.
28. Sánchez-Torres, C., G. S. García-Romo, M. A. Cornejo-Cortés, A. Rivas-Carvalho, and G. Sánchez-Schmitz. 2001. CD16$^+$ and CD16$^-$ human blood monocyte subsets differentiate in vitro to dendritic cells with different abilities to stimulate CD4$^+$ T cells. *Int. Immunol.* 13: 1571–1581.
29. Samaniego, R., B. S. Palacios, A. Domiguez-Soto, C. Vidal, A. Salas, T. Matsuyama, C. Sánchez-Torres, I. de la Torre, M. E. Miranda-Carús, P. Sánchez-Mateos, and A. Puig-Kröger. 2014. Macrophage uptake and accumulation of folates are polarization-dependent in vitro and in vivo and are regulated by activin A. *J. Leukoc. Biol.* 95: 797–808.
30. Wang, J., D. Duncan, Z. Shi, and B. Zhang. 2013. WEB-based GEne SeT AnaLysis Toolkit (WebGestalt): update 2013. *Nucleic Acids Res.* 41(Web Server issue): W77–W83.
31. Subramanian, A., P. Tamayo, V. K. Mootha, S. Mukherjee, B. L. Ebert, M. A. Gillette, A. Paulovich, S. L. Pomeroy, T. R. Golub, E. S. Lander, and J. P. Mesirov. 2005. Gene set enrichment analysis: a knowledge-based approach for interpreting genome-wide expression profiles. *Proc. Natl. Acad. Sci. USA* 102: 15545–15550.
32. Sierra-Filardi, E., C. Nieto, A. Domínguez-Soto, R. Barroso, P. Sánchez-Mateos, A. Puig-Kroger, M. López-Bravo, J. Joven, C. Ardavín, J. L. Rodríguez-Fernández, et al. 2014. CCL2 shapes macrophage polarization by GM-CSF and M-CSF: identification of CCL2/CCR2-dependent gene expression profile. *J. Immunol.* 192: 3858–3867.
33. Sierra-Filardi, E., M. A. Vega, P. Sánchez-Mateos, A. L. Corbí, and A. Puig-Kröger. 2010. Heme oxygenase-1 expression in M-CSF-polarized M2 macrophages contributes to LPS-induced IL-10 release. *Immunobiology* 215: 788–795.
34. Wu, M. F., S. T. Chen, A. H. Yang, W. W. Lin, Y. L. Lin, N. J. Chen, I. S. Tsai, L. Li, and S. L. Hsieh. 2013. CLEC5A is critical for dengue virus-induced inflammasome activation in human macrophages. *Blood* 121: 95–106.
35. Allavena, P., L. Piemonti, D. Longoni, S. Bernasconi, A. Stoppacciaro, L. Ruco, and A. Mantovani. 1998. IL-10 prevents the differentiation of monocytes to dendritic cells but promotes their maturation to macrophages. *Eur. J. Immunol.* 28: 359–369.
36. Domínguez-Soto, A., E. Sierra-Filardi, A. Puig-Kröger, B. Pérez-Maceda, F. Gómez-Aguado, M. T. Corcuera, P. Sánchez-Mateos, and A. L. Corbí. 2011. Dendritic cell-specific ICAM-3-grabbing nonintegrin expression on M2-polarized and tumor-associated macrophages is macrophage-CSF dependent and enhanced by tumor-derived IL-6 and IL-10. *J. Immunol.* 186: 2192–2200.
37. Sica, A., and A. Mantovani. 2012. Macrophage plasticity and polarization: in vivo veritas. *J. Clin. Invest.* 122: 787–795.
38. Han, M. S., D. Y. Jung, C. Morel, S. A. Lakhani, J. K. Kim, R. A. Flavell, and R. J. Davis. 2013. JNK expression by macrophages promotes obesity-induced insulin resistance and inflammation. *Science* 339: 218–222.
39. Sierra-Filardi, E., A. Puig-Kröger, F. J. Blanco, C. Nieto, R. Bragado, M. I. Palomero, C. Bernabéu, M. A. Vega, and A. L. Corbí. 2011. Activin A skews macrophage polarization by promoting a proinflammatory phenotype and inhibiting the acquisition of anti-inflammatory macrophage markers. *Blood* 117: 5092–5101.
40. Domínguez-Soto, A., M. de las Casas-Engel, R. Bragado, J. Medina-Echeverz, L. Aragoneses-Fenoll, E. Martín-Gayo, N. van Rooijen, P. Berraondo, M. L. Toribio, M. A. Moro, et al. 2014. Intravenous immunoglobulin promotes antitumor responses by modulating macrophage polarization. *J. Immunol.* 193: 5181–5189.
41. Escribese, M. M., E. Sierra-Filardi, C. Nieto, R. Samaniego, C. Sánchez-Torres, T. Matsuyama, E. Calderon-Gómez, M. A. Vega, A. Salas, P. Sánchez-Mateos, and A. L. Corbí. 2012. The prolyl hydroxylase PHD3 identifies proinflammatory macrophages and its expression is regulated by activin A. *J. Immunol.* 189: 1946–1954.
42. Lacey, D. C., A. Achuthan, A. J. Fleetwood, H. Dinh, J. Roiniotis, G. M. Scholz, M. W. Chang, S. K. Beckman, A. D. Cook, and J. A. Hamilton. 2012. Defining GM-CSF- and macrophage-CSF-dependent macrophage responses by in vitro models. *J. Immunol.* 188: 5752–5765.
43. Kramer, P. R., V. Winger, and J. Reuben. 2009. PI3K limits TNF-α production in CD16-activated monocytes. *Eur. J. Immunol.* 39: 561–570.
44. Frankenberger, M., T. P. Hofer, A. Marei, F. Dayyani, S. Schewe, C. Strasser, A. Aldraihim, F. Stanzel, R. Lang, R. Hoffmann, et al. 2012. Transcript profiling of CD16-positive monocytes reveals a unique molecular fingerprint. *Eur. J. Immunol.* 42: 957–974.
45. Verreck, F. A., T. de Boer, D. M. Langenberg, L. van der Zanden, and T. H. Ottenhoff. 2006. Phenotypic and functional profiling of human proinflammatory type-1 and anti-inflammatory type-2 macrophages in response to microbial antigens and IFN-γ- and CD40L-mediated costimulation. *J. Leukoc. Biol.* 79: 285–293.
46. Martinez, F. O., S. Gordon, M. Locati, and A. Mantovani. 2006. Transcriptional profiling of the human monocyte-to-macrophage differentiation and polarization: new molecules and patterns of gene expression. *J. Immunol.* 177: 7303–7311.
47. Fleetwood, A. J., H. Dinh, A. D. Cook, P. J. Hertzog, and J. A. Hamilton. 2009. GM-CSF- and M-CSF-dependent macrophage phenotypes display differential dependence on type I interferon signaling. *J. Leukoc. Biol.* 86: 411–421.
48. Tugal, D., X. Liao, and M. K. Jain. 2013. Transcriptional control of macrophage polarization. *Arterioscler. Thromb. Vasc. Biol.* 33: 1135–1144.
49. Xu, H., J. Zhu, S. Smith, J. Foldi, B. Zhao, A. Y. Chung, H. Outtz, J. Kitajewski, C. Shi, S. Weber, et al. 2012. Notch-RBP-J signaling regulates the transcription factor IRF8 to promote inflammatory macrophage polarization. *Nat. Immunol.* 13: 642–650.
50. Ramachandran, P., A. Pellicoro, M. A. Vernon, L. Boulter, R. L. Aucott, A. Ali, S. N. Hartland, V. K. Snowdon, A. Cappon, T. T. Gordon-Walker, et al. 2012. Differential Ly-6C expression identifies the recruited macrophage phenotype, which orchestrates the regression of murine liver fibrosis. *Proc. Natl. Acad. Sci. USA* 109: E3186–E3195.
51. Shechter, R., A. London, C. Varol, C. Raposo, M. Cusimano, G. Yovel, A. Rolls, M. Mack, S. Pluchino, G. Martino, et al. 2009. Infiltrating blood-derived macrophages are vital cells playing an anti-inflammatory role in recovery from spinal cord injury in mice. *PLoS Med.* 6: e1000113.
52. Carlin, L. M., E. G. Stamatiades, C. Auffray, R. N. Hanna, L. Glover, G. Vizcay-Barrena, C. C. Hedrick, H. T. Cook, S. Diebold, and F. Geissmann. 2013. Nr4a1-dependent Ly6C^{low} monocytes monitor endothelial cells and orchestrate their disposal. *Cell* 153: 362–375.
53. Skrzeczyńska-Moncznik, J., M. Bzowska, S. Loseke, E. Grage-Griebenow, M. Zembala, and J. Pryjma. 2008. Peripheral blood CD14^{high} CD16$^+$ monocytes are main producers of IL-10. *Scand. J. Immunol.* 67: 152–159.
54. Barreda, D. R., P. C. Hanington, and M. Belosevic. 2004. Regulation of myeloid development and function by colony stimulating factors. *Dev. Comp. Immunol.* 28: 509–554.
55. Maeshima, K., A. Maeshima, Y. Hayashi, S. Kishi, and I. Kojima. 2004. Crucial role of activin A in tubulogenesis of endothelial cells induced by vascular endothelial growth factor. *Endocrinology* 145: 3739–3745.
56. Poulaki, V., N. Mitsiades, F. E. Kruse, S. Radetzky, E. Iliaki, B. Kirchhof, and A. M. Joussen. 2004. Activin A in the regulation of corneal neovascularization and vascular endothelial growth factor expression. *Am. J. Pathol.* 164: 1293–1302.

SUPPLEMENTAL INFORMATION

Atypical activin A and IL-10 production impairs human CD16^{+} monocyte differentiation into anti-inflammatory macrophages

Érika González-Domínguez, Ángeles Domínguez-Soto, Concha Nieto, José Luis Flores-Sevilla, Mariana Pacheco-Blanco, Victoria Campos-Peña, Marco A. Meraz-Ríos, Miguel A. Vega, Ángel L. Corbí, and Carmen Sánchez-Torres

Supplemental Figure 1

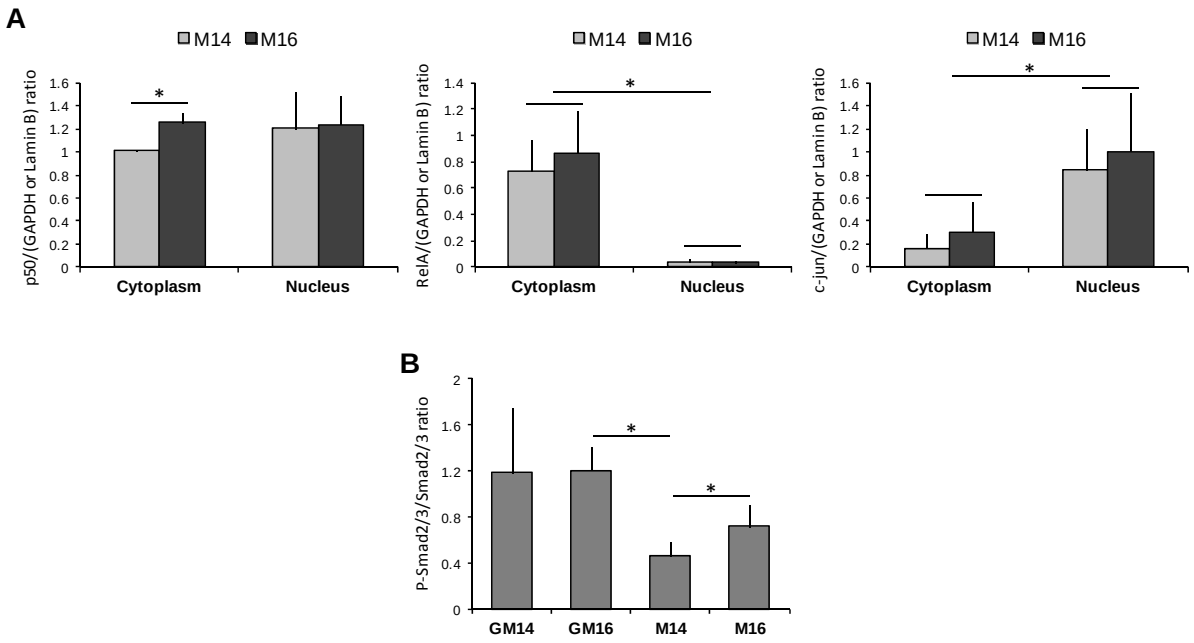

Supplemental Figure 1. (A) Densitometric analysis of p50, RelA and c-jun expression in cytoplasmic and nuclear extracts from M14 and M16 differentiated for 6 days. The results are related to Figure 2D, and represent the mean ± SD of the ratios between the density of p50, RelA or c-jun bands and the density of GAPDH (cytoplasm) or Lamin B (nucleus) bands in 3-4 separate donors. (B) Densitometric analysis of p-Smad2/3 and Smad2/3 in protein extracts from GM14, GM16, M14 and M16 differentiated for 6 days. The results are related to Figure 5B, and represent the mean ± SD of the ratios between the density of p-Smad2/3 bands and the density of Smad2/3 bands in 4 independent donors. Statistics were performed with the paired *t* test. *$p < 0.05$.

Supplemental Figure 2

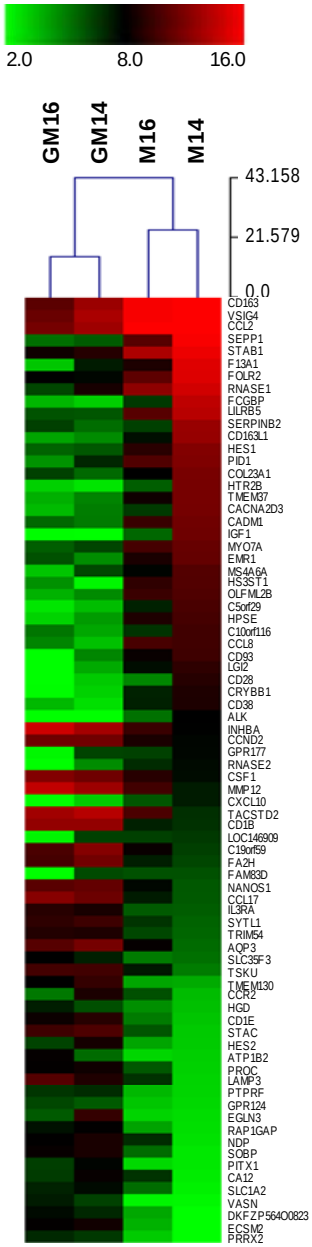

Supplemental Figure 2. Microarray analysis of transcript expression in GM14, GM16, M14 and M16. Average expression of the top 25 genes up-regulated in GM14 *vs* M14 and in GM16 *vs* M16 (38 genes), as well as the top 25 genes up-regulated in

M14 *vs* GM14 and in M16 *vs* GM16 (40 genes), depicted as heat maps. The normalized mean values (log_2) of these genes were subjected to a non-supervised hierarchical clustering (HLC) on the MultipleExperiment Viewer (MeV) software, using the average linkage clustering method and the Euclidean distance metric.

Supplemental Figure 3

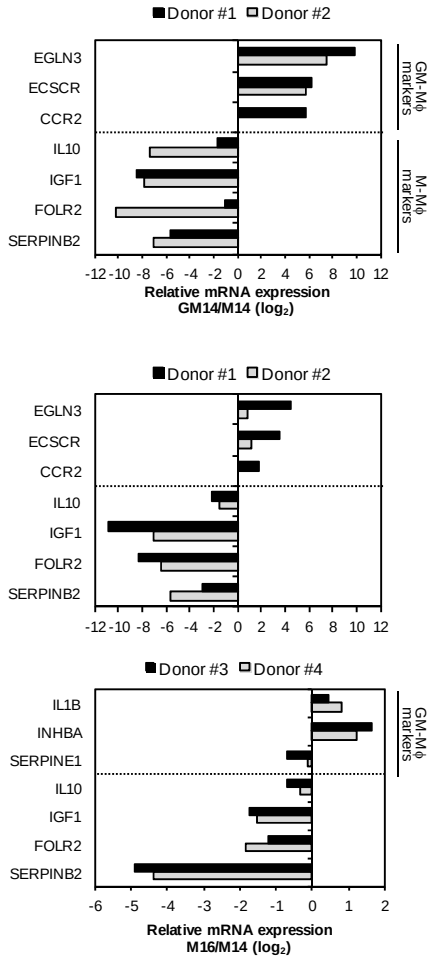

Supplemental Figure 3. Relative expression of selected GM- and M-Mf-associated polarization genes in M14 and M16. Relative expression (log_2) of the indicated GM- and M-Mϕ-associated genes determined by qRT-PCR in M14 and M16, as well as in GM14 as a control. Results of the top and middle panels correspond to two separate donors and are depicted as relative mRNA expression (relative to *TBP* mRNA levels) of each gene in GM14 (top) or M16 (middle) and referred to the expression levels detected in M14. The bottom panel represents the results of two additional donors showed as

relative mRNA expression (relative to *TBP* mRNA levels) of each gene in M16 with respect to the expression in M14.

Supplemental Figure 4

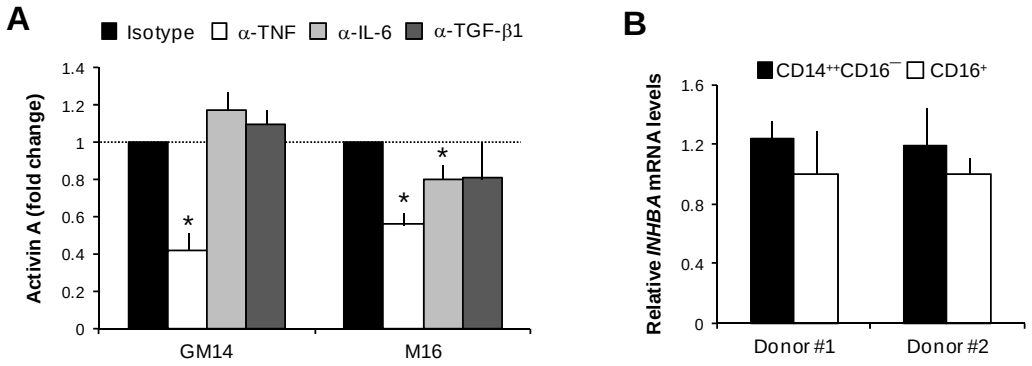

Supplemental Figure 4. Activin A secretion by M16 is dependent on TNF and is not an intrinsic property of their monocyte precursors. (A) GM14 (as a control) and M16 were cultured for two days in the presence of neutralizing mAbs against TNF, IL-6, TGF-β1, or isotype-matched irrelevant mAbs. Culture SNs were harvested and analyzed for activin A levels by ELISA. The results are shown as the fold change of activin A production in the presence of blocking antibodies relative to their production with Igs control. The values represent the mean ± SD of 3 donors evaluated. (B) Expression of *INHBA* mRNA levels in freshly isolated blood $CD14^{++}CD16^{-}$ and $CD16^{+}$ monocytes from two separate donors, evaluated by qRT-PCR and relative to *TBP* mRNA levels. Each determination was done in triplicate, and results represent the mean ± SD of triplicates.